Available online at www.sciencedirect.com

SciVerse ScienceDirect

Ceramics International 39 (2013) 8113–8121

CERAMICS INTERNATIONAL

www.elsevier.com/locate/ceramint

High temperature dielectric and magnetic response of Ti and Pr doped $BiFeO_3$ ceramics

Virendra Kumar[a], Anurag Gaur[a,*], Neha Sharma[a], Jyoti Shah[b], R.K. Kotnala[b]

[a]*Department of Physics, National Institute of Technology, Kurukshetra 136119, India*
[b]*National Physical Laboratory, Dr. K.S. Krishnan Marg, New Delhi 110012, India*

Received 31 January 2013; received in revised form 21 March 2013; accepted 25 March 2013
Available online 6 April 2013

Abstract

In the present study, four different compositions of Ti and Pr doped $BiFeO_3$ samples were synthesized by conventional rapid liquid phase sintering and their structural, dielectric, ferroelectric and magnetic properties were investigated. High temperature dielectric study shows different anomalous response for all compositions. A major peak in dielectric constant versus temperature curve is observed at 640 K for pristine $BiFeO_3$ which shifts to 545 K for Ti doped ($BiFe_{0.9}Ti_{0.1}O_3$) sample. Moreover, multiple peaks are observed for Pr doped ($Bi_{0.9}Pr_{0.1}FeO_3$) sample in temperature range of 400–800 K. The room temperature P–E loop study shows that the value of maximum polarization increases from 0.185 to 0.859 μC/cm^2 for Pr doped ($Bi_{0.9}Pr_{0.1}FeO_3$) sample and also increases the ability of $BiFeO_3$ to withstand higher electric field. Room temperature magnetic (*M–H*) curve shows a slight increment in the value of magnetization from 0.071 to 0.078 emu/gm for pristine $BiFeO_3$ to Pr and Ti co-doped $Bi_{0.9}Pr_{0.1}Fe_{0.9}Ti_{0.1}O_3$, respectively.

Keywords: Multiferroic; Dielectrics; Antiferromagnetism

1. Introduction

Extensive research efforts on magneto-electrics in recent years have stimulated the exploration of these properties in many materials and revived the investigation of known compounds, among which Bismuth ferrite ($BiFeO_3$) stands out as an unique example. The reason for $BiFeO_3$ occupying a center stage among magneto-electrics or multiferroic materials is due to its two ferroic orders (antiferromagnetic and ferroelectric) which coexist at room temperature [1]. $BiFeO_3$ apart from showing coexistence of two ferroic orders at room temperature also exhibits photovoltaic effect, metal-insulation transition, electric modulation of conduction and terahertz radiation emission. Due to nontoxic composition and above room temperature multifunctionality, it becomes potential material for wide variety of applications such as sensors, memories and spintronic devices [2]. $BiFeO_3$ has a very high electric polarization below its Curie temperature $T_c = 1143$ K and shows antiferromagnetic nature below $T_N = 643$ K. The room temperature phase of $BiFeO_3$ is classed as rhombohedral (point group R3c). The perovskite type unit cell has a lattice parameter a_{rh} of 3.965 Å and rhombohedral angle α_{rh} 89.3° at room temperature with ferroelectric polarization along $[111]_{Pseudocubic}$ [3]. $BiFeO_3$ is known to exhibit a spin cycloid structure in the bulk. The spins which form a cycloid structure are having a wavelength of $\lambda_o = 62$ nm and associated cycloid wave vector equal to $Q = 2\pi/\lambda_o$ [4]. An electric field can simultaneously induce the flip of polarization and the cycloidal plane. The electrical switch of antiferromagnetic–ferroelectric domains in $BiFeO_3$ has been observed and controlled in a ferromagnet-multiferroic hetrostructures [5,6]. Synthesis of pure $BiFeO_3$ as bulk, as well as nanoparticles, is a challenging task due to its narrow temperature range phase stabilization and kinetics of phase formation in Bi_2O_3 [6,7]. High leakage current is another major problem associated with this compound, which is generally responsible for its inferior ferroelectric behavior. Leakage current problem is mainly attributed to the existence of smaller number of Fe^{+3} ions and oxygen vacancies [8]. The cycloidal structure is responsible for the disappearance of weak ferromagnetism and the linear magneto-electric (M-E) effect due to averaging over the period.

*Corresponding author. Tel.: +91 1744 233549; fax: +91 1744 238050.
E-mail address: anuragdph@gmail.com (A. Gaur).

0272-8842/$ - see front matter © 2013 Elsevier Ltd and Techna Group S.r.l. All rights reserved.
http://dx.doi.org/10.1016/j.ceramint.2013.03.084

Doping is generally considered to be an effective way to suppress the cycloidal structure of $BiFeO_3$ and to increase its magnetic behavior and M-E effect up to some extent. Apart from this doping is also considered an effective way to improve leaky ferroelectric behavior of this compound [9]. Generally, doping of Lanthanide element at Bi site and transition element at Fe site increases magnetization [10,11]. It has also been reported that Ti doping at Fe site reduces the leakage current and improves the ferroelectric properties of the $BiFeO_3$ [12,13]. Due to all these findings, in the present study, we have planned to dope $BiFeO_3$ by rare earth Pr ion at Bi site and Ti at Fe site. To best of our knowledge, this unique combination of Pr and Ti doping in $BiFeO_3$ at Bi and Fe sites, respectively, have not been studied earlier. We synthesized four different compositions of pure and doped $BiFeO_3$ e.g. pristine $BiFeO_3$, Ti doped ($BiFe_{0.9}Ti_{0.1}O_3$), Pr doped ($Bi_{0.9}Pr_{0.1}FeO_3$), and Pr and Ti co-doped ($Bi_{0.9}Pr_{0.1}Fe_{0.9}Ti_{0.1}O_3$) by rapid liquid phase sintering and studied their structural, high temperature dielectric and magnetic behavior.

2. Experimental

Pristine $BiFeO_3$, Ti doped ($BiFe_{0.9}Ti_{0.1}O_3$), Pr doped ($Bi_{0.9}Pr_{0.1}FeO_3$), and Pr and Ti co-doped ($Bi_{0.9}Pr_{0.1}Fe_{0.9}Ti_{0.1}O_3$) samples were prepared by rapid liquid phase sintering. High purity powders of Pr_2O_3, Bi_2O_3, Fe_2O_3 and TiO_2 were weighted in stoichiometric proportion and ground for an hour in a pestle motor and finally fired in air at 880 °C for 450 s. High temperature furnace having high heating rate of 100 °C/s was used for sintering. After rapid sintering, the sample was cooled in air [13]. The cooled mixture was further ground and leached in dilute HNO_3 followed by washing in distill water. Washed extract was dried and pelletized by a dye of 8 mm diameter and heated at 650 °C for 1.25 h. Phase composition of the prepared samples were checked by X-ray diffractometer (RIGAKU) with Cukα radiation of $\lambda = 1.54056$ Å and scan speed of 0.2/min for 2θ range between 20 and 80°. The microstructure of the samples was examined with scanning electron microscopy (SEM) and magnetization measurement with temperature variations were done by using vibration sample magnetometer (Lakeshore VSM 7304). The dielectric measurements were carried out on silver coated pellets by using N4L-LCR meter (Model: 1735) and ferroelectric hysteresis loops were measured by using ferroelectric loop tracer based on Sawyer–Tower circuit. Second order magnetoelectric effect was observed and consequently second order magnetoelectric coefficient β was calculated with the help of home-made experimental setup as reported by Kumar et al. [14].

3. Results and discussion

Fig. 1(a) presents the XRD pattern of $BiFeO_3$, $BiFe_{0.9}Ti_{0.1}O_3$, $Bi_{0.9}Pr_{0.1}FeO_3$ and $Bi_{0.9}Pr_{0.1}Fe_{0.9}Ti_{0.1}O_3$ samples. The XRD pattern confirms the single phase formation of $BiFeO_3$ for all samples without any impurity phase. Furthermore, splitting of diffraction peaks at 22° and 45° are not observed for doped samples as reported by Cui et al. [13] for La and Ti co-doped $BiFeO_3$. This indicates that there is no phase transition from rhombohedral to tetragonal for Pr and Ti co-doped $BiFeO_3$ as reported by others [15,16]. Moreover, Rietveld refinement, performed on the XRD data of pristine $BiFeO_3$, is presented in Fig. 1(b). Fig. 1(b) features the observed, calculated and difference XRD profiles of pristine $BiFeO_3$ after final cycle of refinement. It is noticed that the observed and calculated profiles correspond to each other. The Rietveld refinement was carried out by considering R3c space group with ionic positions of Bi at 6a, Fe at 6a and O at 18b [17]. The Bragg peaks were modeled with Thompson–Cox–Hastings pseudo-Voigt function and the background was estimated by linear interpolation between selected background points. The lattice parameters calculated through refinement for pristine $BiFeO_3$ are $a = b = 5.63184$ Å, and $c = 13.99974$ Å.

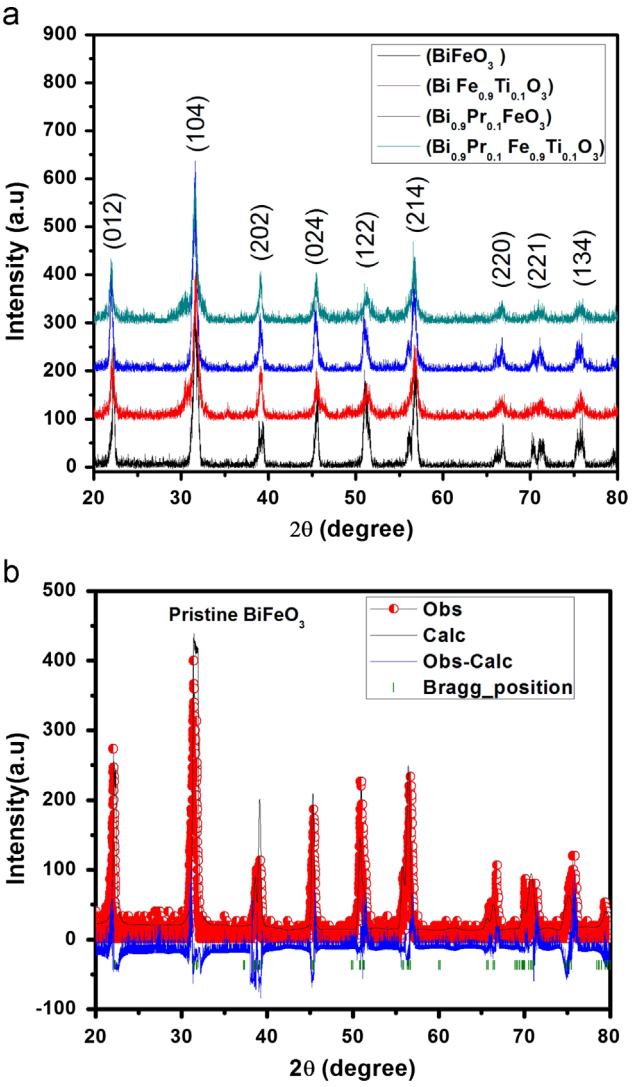

Fig. 1. (a): X-ray diffraction patterns of $BiFeO_3$, $BiFe_{0.9}Ti_{0.1}O_3$, $Bi_{0.9}Pr_{0.1}FeO_3$ and $Bi_{0.9}Pr_{0.1}Fe_{0.9}Ti_{0.1}O_3$ samples. (b): Rietveld refinement pattern of pristine $BiFeO_3$.

The SEM micrographs of all studied samples are presented in Fig. 2(a–d). Micrographs show that grains are of non-uniform shape and size with intergranular porosity, which

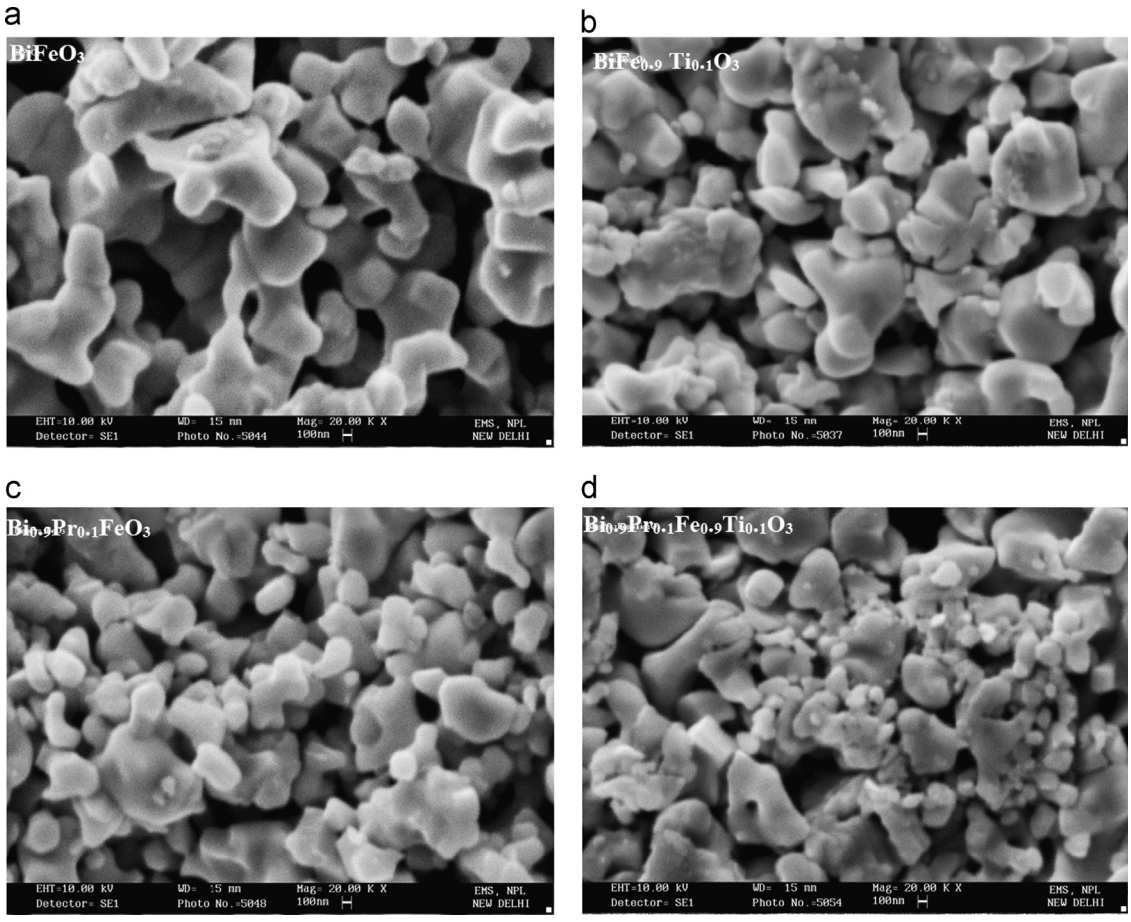

Fig. 2. (a–d): Scanning electron micrographs of $BiFeO_3$, $BiFe_{0.9}Ti_{0.1}O_3$, $Bi_{0.9}Pr_{0.1}FeO_3$ and $Bi_{0.9}Pr_{0.1}Fe_{0.9}Ti_{0.1}O_3$ samples.

affects the sample density. However, intergranular porosity is observed for all samples but it is quite high in case of pristine $BiFeO_3$ due to Kirkendall effect, which arises due to different diffusion rates of constituting elements of $BiFeO_3$. Furthermore, porosity decreases for doped $BiFeO_3$ ($Bi_{0.9}Pr_{0.1}FeO_3$, $BiFe_{0.9}Ti_{0.1}O_3$ and $Bi_{0.9}Pr_{0.1}Fe_{0.9}Ti_{0.1}O_3$) due to dilution of Kirkendall effect after doping. The doped particles are inert markers to main diffusion process of Bi, Fe and O_2, which creates hindrance to the rate of diffusion process by reducing the value of diffusion coefficient and hence diluting the Kirkendall effect [18].

Dielectric constant variation with temperature at different frequencies (10^3–10^6 Hz) is depicted in Fig. 3(a–d), which shows that a major peak in dielectric behavior is observed at 640 K for pristine $BiFeO_3$ which shifts to 545 K for Ti doped ($BiFe_{0.9}Ti_{0.1}O_3$). Moreover, multiple peaks are observed for Pr doped ($Bi_{0.9}Pr_{0.1}FeO_3$) in the temperature range of 400–800 K. The reason for observation of these multipeaks may be the outcome of combined non-Debye and Maxwell–Wagner relaxation effect. Interestingly, no peak is observed for Ti and Pr co-doped ($Bi_{0.9}Pr_{0.1}Fe_{0.9}Ti_{0.1}O_3$) composition, which indicates the reduction of ferroelectric nature and suppression of relaxation behavior in this composition above room temperature. However, the ferroelectric nature of this sample at room temperature slightly improves as indicated by P–E loop study in Fig. 7.

The occurrence of these peaks in dielectric behavior for $BiFeO_3$, $BiFe_{0.9}Ti_{0.1}O_3$ and $Bi_{0.9}Pr_{0.1}FeO_3$ samples may be attributed to the dielectric relaxation process superimposed with electrode interface polarization. Relaxation behavior up to the temperature range of 400 K and at higher frequencies can be explained on the basis of non-Debye dielectric spectrum, which is observed for Pr doped ($Bi_{0.9}Pr_{0.1}FeO_3$) by getting the peak at 400 K. This non-Debye dielectric effect can be described by the Havriliak–Negami relationship

$$\varepsilon^*(\omega) = \frac{\varepsilon_s - \varepsilon_\infty}{[1 + (i\omega\tau_m)^\alpha]^\beta} \quad 0 \le \alpha, \beta \le 1$$

where $\varepsilon^*(\omega)$ is the complex dielectric permittivity at ω angular frequency and ε_s,ε_∞ are low and high frequency limits of dielectric permittivity and τ_m represents characteristic relaxation time. The specific case $\alpha=1$ and $\beta=1$ gives the Debye relaxation law, the case $\beta=1$, $\alpha\neq1$ corresponds to the so called Cole–Cole equation and the case $\alpha=1$, $\beta\neq1$ represents the Cole–Davidson formula.

Furthermore, the Maxwell–Wagner relaxation effect is known to be a main reason for the occurrence of peaks in dielectric behavior at a temperature range of above 400 K as observed in all samples except for Ti and Pr co-doped ($Bi_{0.9}Pr_{0.1}Fe_{0.9}Ti_{0.1}O_3$) composition where no peak is observed. Maxwell–Wagner relaxation effect generally refers to interfacial polarization which occurs when electric current

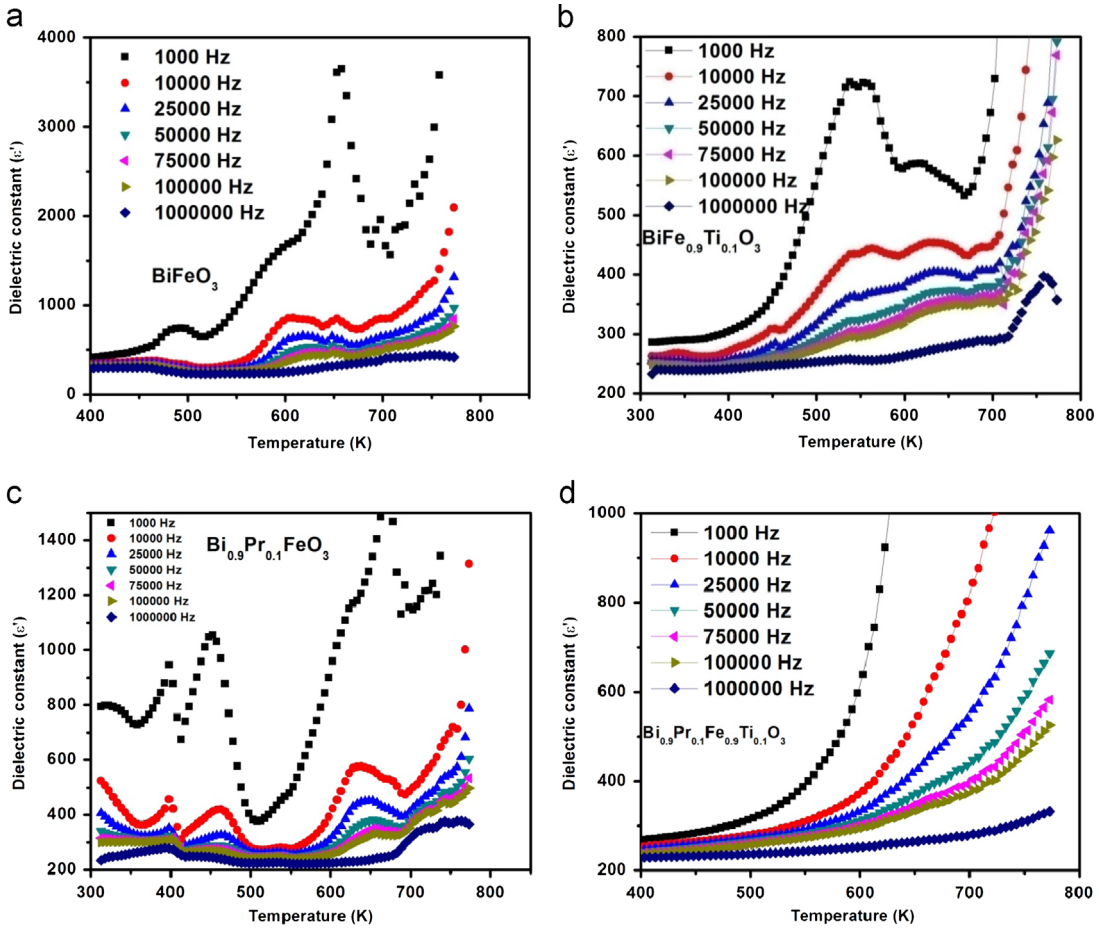

Fig. 3. (a–d): Dielectric constant (ε') versus temperature plots of $BiFeO_3$, $BiFe_{0.9}Ti_{0.1}O_3$, $Bi_{0.9}Pr_{0.1}FeO_3$ and $Bi_{0.9}Pr_{0.1}Fe_{0.9}Ti_{0.1}O_3$ samples at different frequencies.

passes through interfaces between two different media, having different conductivities, which lead to surface charges pileup at the interfaces and give rise to the Debye like relaxation process under an external alternating voltage [19]. The relaxation time of Maxwell–Wagner effect is determined by the product of resistance of the grains R_g and capacitance of the grain boundaries C_{gb}. Therefore, distribution of grain size and inhomogeneous conductivity of the grains may cause a distribution of relaxation times τ and lead to broader relaxation peaks. The effective dielectric permittivity of the sample at frequencies much lower than the relaxation frequency $1/2\pi\tau$ can be approximated from the relation $\varepsilon = C_{gb}/C_o$, where C_{gb} is the capacity at grain boundaries and C_o is the vacuum capacitance of the sample. Piling of charges at grain boundaries will significantly increase the value of C_{gb}, which will turn the increase in value of ε. This enhancement in the value of ε will eventually result in the peak formation [20].

Dielectric loss versus temperature curves recorded at a frequency range (10^3–10^6 Hz) are presented in Fig. 4(a–d). A major peak in dielectric loss behavior is observed at 700 K for pristine $BiFeO_3$, which is reduced to 313 K for Ti doped $BiFe_{0.9}Ti_{0.1}O_3$. Furthermore, this peak is observed at 750 K for Pr doped $Bi_{0.9}Pr_{0.1}FeO_3$. Moreover, no peak is observed for Ti and Pr co-doped $Bi_{0.9}Pr_{0.1}Fe_{0.9}Ti_{0.1}O_3$ just like in the dielectric constant behavior. The reason for occurrence of loss peaks can be again correlated to non-Debye relaxation and Maxwell–Wagner effect as explained above in dielectric constant part.

Variation of dielectric constant and dielectric loss with frequency taken on a log scale for all samples at room temperature is shown in Figs. 5 and 6, respectively. It is observed that the value of dielectric constant decreases by the doping of Ti and Pr at lower frequencies. In our case, the value of dielectric constant is maximum for pristine $BiFeO_3$ and minimum for Pr and Ti co-doped $Bi_{0.9}Pr_{0.1}Fe_{0.9}Ti_{0.1}O_3$, which may be attributed to decreased space charge relaxation at interface and reduced conductivity after doping, as reported by others [21,22]. However, the value of dielectric constant is almost same for all four samples at higher frequencies. At lower frequencies, dielectric constant no longer remains intrinsic property of the ceramic rather it is related to conductivity and inhomogeneity of the ceramic apart from the interface charge relaxation. The space charges are suggested to originate from O^{2+} and Bi^{3+}. After doping, oxygen vacancies will be reduced due to the requirement of charge compensation and this will eventually decrease space charge relaxation behavior. Similarly, the dielectric loss plotted with frequency at room temperature also shows decrement in the value of dielectric loss with increasing frequency and its value is maximum for pristine $BiFeO_3$ which decreases for doped samples as observed through dielectric constant results.

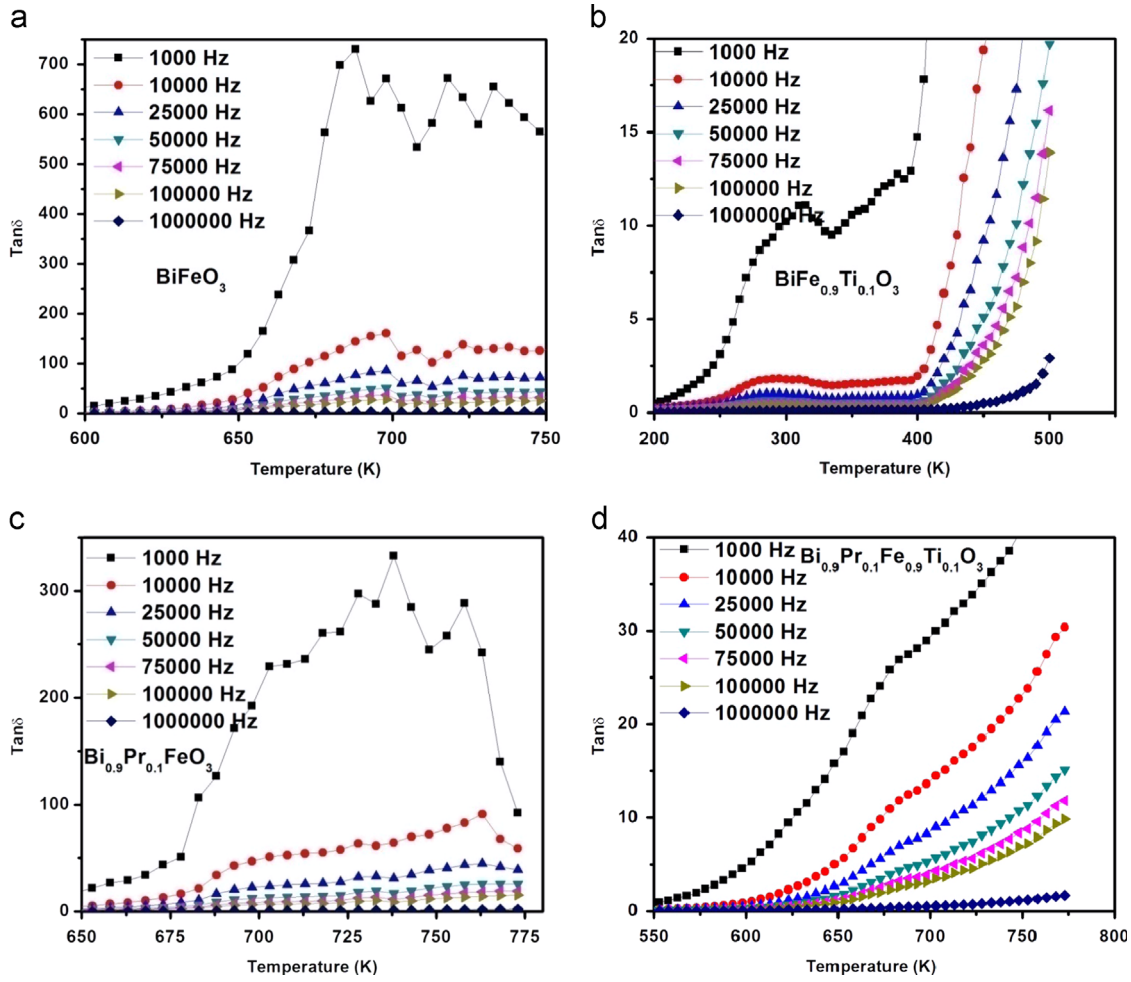

Fig. 4. (a-d): Dielectric loss (tan δ) versus temperature plots of $BiFeO_3$, $BiFe_{0.9}Ti_{0.1}O_3$, $Bi_{0.9}Pr_{0.1}FeO_3$ and $Bi_{0.9}Pr_{0.1}Fe_{0.9}Ti_{0.1}O_3$ at different frequencies.

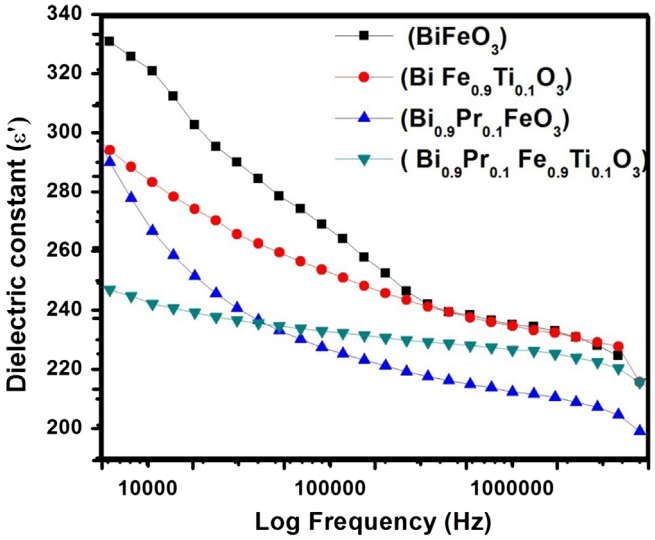

Fig. 5. Dielectric constant (ε') versus frequency plots of $BiFeO_3$, $BiFe_{0.9}Ti_{0.1}O_3$, $Bi_{0.9}Pr_{0.1}FeO_3$ and $Bi_{0.9}Pr_{0.1}Fe_{0.9}Ti_{0.1}O_3$ samples at room temperature.

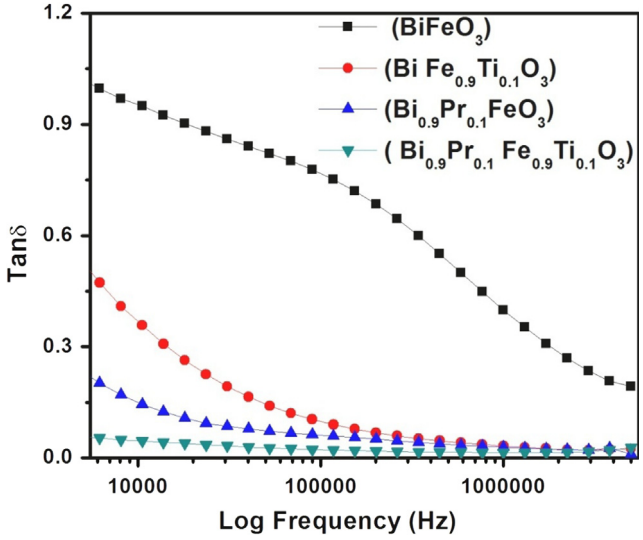

Fig. 6. Dielectric loss (tan δ) versus frequency plots at room temperature of $BiFeO_3$, $BiFe_{0.9}Ti_{0.1}O_3$, $Bi_{0.9}Pr_{0.1}FeO_3$ and $Bi_{0.9}Pr_{0.1}Fe_{0.9}Ti_{0.1}O_3$.

Ferroelectric study carried out by P–E loop tracer for all samples poled at 40 °C under the constant electric field of 0.6 kV is depicted in Fig. 7. Pure $BiFeO_3$ exhibits leaky ferroelectric behavior and is not able to withstand applied electric field more than 2 kV due to large leakage current. Maximum value of polarization for pure $BiFeO_3$ is 0.18 μC/cm^2, which

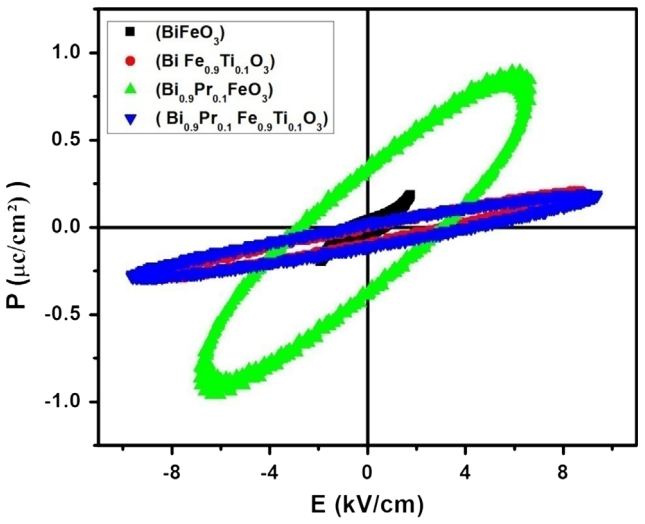

Fig. 7. Polarization versus electric field (P–E) loops at room temperature of $BiFeO_3$, $BiFe_{0.9}Ti_{0.1}O_3$, $Bi_{0.9}Pr_{0.1}FeO_3$ and $Bi_{0.9}Pr_{0.1}Fe_{0.9}Ti_{0.1}O_3$ samples.

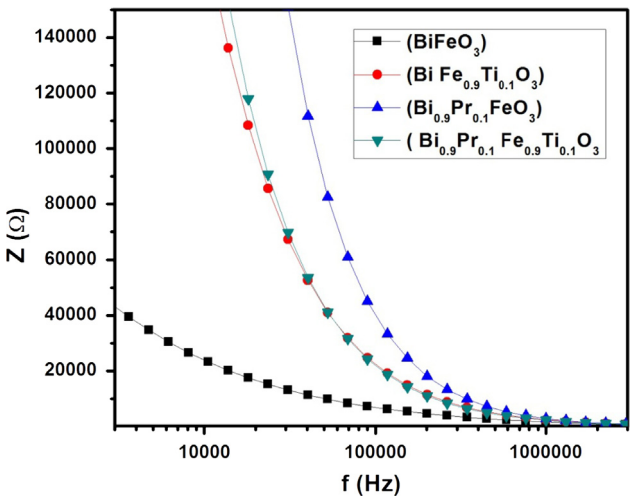

Fig. 8. Impedance versus frequency (*Z–f*) loops at room temperature of $BiFeO_3$, $BiFe_{0.9}Ti_{0.1}O_3$, $Bi_{0.9}Pr_{0.1}FeO_3$ and $Bi_{0.9}Pr_{0.1}Fe_{0.9}Ti_{0.1}O_3$ samples.

significantly enhances to 0.859 μC/cm^2 for Pr doped sample. The reason for this enhancement may be the replacement of volatile Bi ions in $BiFeO_3$ by Pr ions which reduces the concentration of oxygen vacancies, which are mainly responsible for its poor ferroelectric behavior. Pr doping also increases the ability of $BiFeO_3$ to withstand higher electric field up to the order of 6 kV as observed from Fig. 7. Furthermore, the value of maximum polarization increases up to 0.21 μC/cm^2 for Ti doped sample. The reason for this may be the doping of Ti at Fe site, which will reduce the concentration of Fe ions, which have variable oxidation states (Fe^{2+}, Fe^{3+}) and considered to be responsible for oxygen vacancies. The value of maximum polarization for Ti and Pr co-doped sample is almost equal to pristine $BiFeO_3$ that is 0.19 μC/cm^2. This indicates that there is no significant change in concentration of oxygen after co-doping of Pr and Ti [23].

Fig. 8 represents the variation of real part of impedance *Z* as a function of frequency at room temperature for all samples. The pattern shows a sigmoidal variation as a function of frequency in low frequency region followed by a saturated region in high frequency region. This indicates the mixed nature of polarization behavior in the material. The pattern shows a very steep *Z* dispersion in the low frequency region of the spectrum. The extent of steepness in the low frequency region is observed to have a very strong dependence of *Z* on the composition of $BiFeO_3$. At lower frequency, impedance is minimum for the pristine $BiFeO_3$ and maximum for Pr doped $Bi_{0.9}Pr_{0.1}FeO_3$ sample. The reason for this may be its enhanced ferroelectric behavior after Pr doping as observed from P–E loop results from Fig. 7. Furthermore, Ti doped $BiFe_{0.9}Ti_{0.1}O_3$ and Ti and Pr co-doped $Bi_{0.9}Pr_{0.1}Fe_{0.9}Ti_{0.1}O_3$ sample curves overlap, however, the value of impedance is higher as compared to pure $BiFeO_3$. This may be again attributed to slight improved ferroelectric nature after Ti and Ti, Pr co-doping as observed in Fig. 7.

Fig. 9(a–d) represents the magnetization versus field (*M–H*) behavior of all samples at room temperature. Pristine $BiFeO_3$ sample shows antiferromagnetic behavior at room temperature. However, the value of magnetization increases slightly by the doping of Ti, and Pr. Peculiar shaped loops are observed for doped samples particularly for Ti doped and Ti, Pr co-doped samples. The reason for observation of such loops may be the magnetic interaction between Fe^{+3}–Ti^{+3} and Fe^{+3}–Pr^{+3} ions. The combined effect of these two interactions give butterfly shaped loop observed for Ti, Pr co-doped sample which indicates the existence of weak ferromagnetism in this sample [24,25]. The value of magnetization is 0.071 emu/g for pristine $BiFeO_3$ which further increases to 0.078 emu/g for Ti, Pr co-doped sample. The magnetic order of this ceramic is little complicated with ferromagnetic coupling within a plane and antiferromagnetic coupling between two adjacent planes. Due to antisymmetric Dzyaloshinsky–Moriya (DM) exchange interaction, canted antiferromagnetism may develop. However, a spiral spin structure is superimposed on this antiferromagnetic order in which the antiferromagnetic axis is rotated through the crystal and develops an incommensurate order. Moreover $BiFeO_3$ exhibit canted spin G type antiferromagnetic structure and this G type structure is modified by the long range modulation of the cycloidal spiral with the [110] spiral direction. The cycloidal structure results in the disappearance of the weak ferromagnetism due to averaging over the period. Ti, Pr doping and Ti, Pr co-doping can induce the change in cycloidal spin structure so the latent magnetization within the cycloid is released. This can be accounted for increase in magnetization after doping [26–28].

Fig. 10 represents magnetization versus temperature curves for all samples at 1000 Oe. Multiple kinks or anomalous points are observed in *M–T* curve for all the compositions. These multiple kinks cannot be attributed to antiferromagnetic–paramagnetic phase transition but are generally believed to originate from the ordering of Bi^{3+} and Fe^{3+} ions and oxygen vacancies, which induce electrons transfer from Fe^{2+} to Bi^{3+} ion and creates intermediate spin Fe^{3+} and Jahn–Teller Bi^{5+} ions. Doping of Pr at Bi site significantly increases the Jahn–Teller interaction

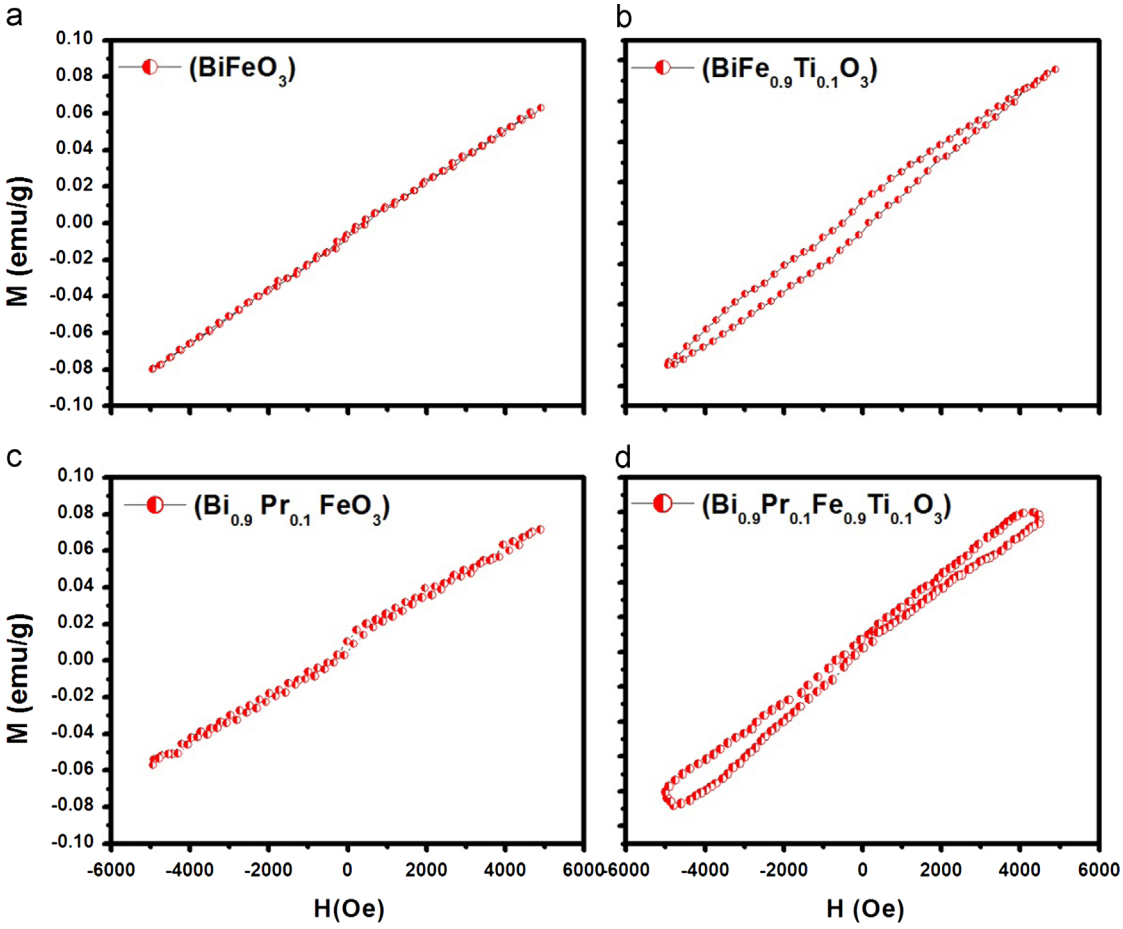

Fig. 9. Magnetization versus magnetic field (M–H) plots at room temperature of $BiFeO_3$, $BiFe_{0.9}Ti_{0.1}O_3$, $Bi_{0.9}Pr_{0.1}FeO_3$ and $Bi_{0.9}Pr_{0.1}Fe_{0.9}Ti_{0.1}O_3$ samples.

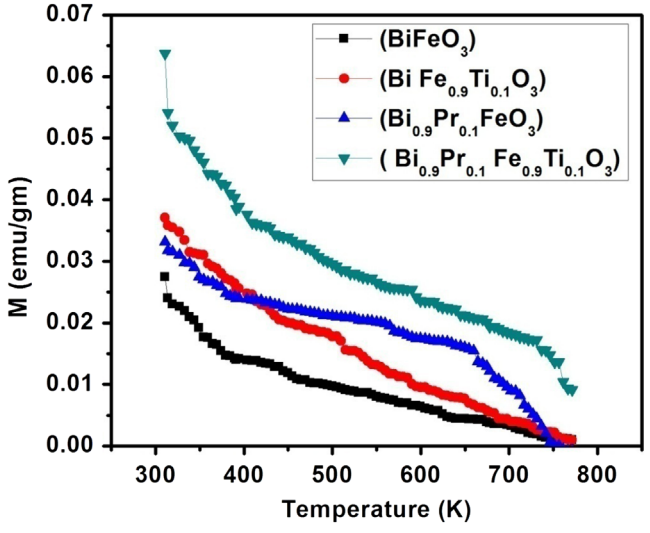

Fig. 10. Magnetization versus temperature (M–T) plots at 1000 Oe field for $BiFeO_3$, $BiFe_{0.9}Ti_{0.1}O_3$, $Bi_{0.9}Pr_{0.1}FeO_3$ and $Bi_{0.9}Pr_{0.1}Fe_{0.9}Ti_{0.1}O_3$.

between two ions, due to this Pr doped sample which exhibits unusual enhanced magnetization in M–T measurement [29,30]. Moreover magnetic inhomogeneity and weak Dzyaloshinskii–Moriya type interaction can also be responsible for this joint coexistence of weak ferromagnetic and antiferromagnetic phases [25].

For obtaining the second order quadratic ME coefficient (β_{111}), the dynamic measurement experiment was performed as given by Kumar et al. [14]. In the dynamic measurement method, the output ME voltage is measured with a bias ac magnetic field while keeping the quasi-static measurement in act i.e. the measurement is carried out with a time varying dc magnetic field in the presence of an ac field. When dc magnetic field is applied, ME output voltage (V) in a material, showing second-order effect can be given by the following equation $V \propto (\alpha H + \beta H.H)$, where α and β are the coefficients of linear and quadratic components of ME effect. Suppose that if an ac field (h_o) is superimposed over dc field (H_o), then effective field is $H = H_o + h_o \sin(\omega t)$. A lock-in-amplifier tuned to the frequency $\omega(\omega = 2\pi f)$ to measure the output ME signal. Keeping the dc magnetic field zero, with increasing ac field, the ME signal can be recorded which gives linear Magneto-electric coefficient (α). In our case, we could not get any variation in ME signal with varying ac field (h_o) under zero dc field (H_o), which indicates that the linear ME coefficient α (α_{ik}) cannot be observed for our samples. Then by properly selecting a fixed value of ac field (5 Oe in our case), the dc field was swept using the stepper motor through computer. The induced ME output voltage signal in the sample was measured

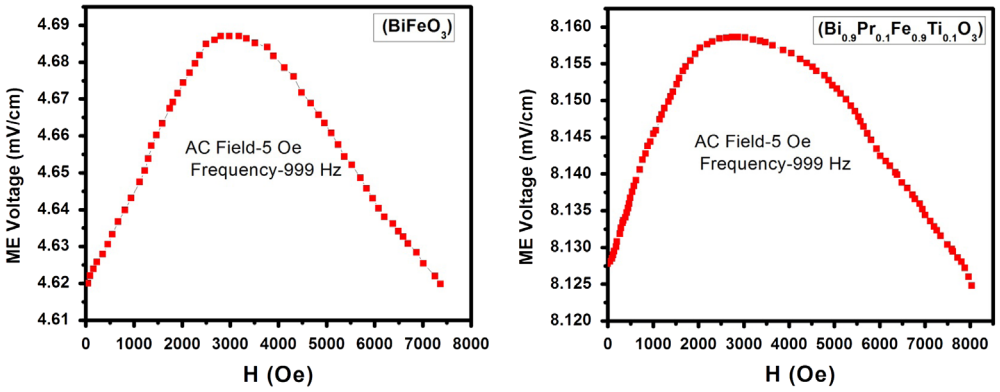

Fig. 11. Magneto-electric voltage signal versus magnetic field plots at room temperature of $BiFeO_3$ and $Bi_{0.9}Pr_{0.1}Fe_{0.9}Ti_{0.1}O_3$.

with the lock-in amplifier keeping its frequency at 500 Hz. For measuring the value of β_{111} (hence forth indicated as β), all the samples were electrically poled for 2 h under constant electric field of 1 kV before the measurement.

In Fig. 11(a and b) variation of ME output voltage with applied DC magnetic field in the presence of constant AC magnetic field of 5 Oe and frequency 500 Hz is presented. For $BiFeO_3$ and Ti, Pr co-doped $Bi_{0.9}Pr_{0.1}Fe_{0.9}Ti_{0.1}O_3$ samples, typical parabola shape curves are obtained, which are considered to be a conclusive evidence of ME coupling. With the help of ME output voltage curve plotted with varying dc field, the average quadratic second order ME coefficient β was calculated by substituting the value of $\alpha=0$ in the mathematical relation given above. The average value of β obtained from the figure is 12.25×10^{-5} mV/cm Oe^2 for pristine $BiFeO_3$ and 34.72×10^{-5} mV/cm Oe^2 for Ti, Pr co-doped $Bi_{0.9}Pr_{0.1}Fe_{0.9}Ti_{0.1}O_3$. The reason for enhancement in the value of β for Ti, Pr co-doped $Bi_{0.9}Pr_{0.1}Fe_{0.9}Ti_{0.1}O_3$ may be attributed to the observed enhancement in the value of room temperature magnetization and polarization since in single phase multiferroics, ME output arises due to the interaction between magnetic and ferroelectric sub-lattices [14].

4. Conclusions

Four different compositions of Ti and Pr doped $BiFeO_3$ ceramics samples were prepared by rapid liquid phase sintering. Dielectric curves plotted at different frequencies against high temperature show a peak in dielectric behavior at 640 K for pristine $BiFeO_3$ which shifts to 545 K for Ti doped ($BiFe_{0.9}Ti_{0.1}O_3$). Moreover, multiple peaks are observed for Pr doped ($Bi_{0.9}Pr_{0.1}FeO_3$) in temperature range of 400–800 K, which indicates its improved ferroelectric behavior which is also supported by its P–E loop study. Moreover, no peak is observed for Ti and Pr co-doped ($Bi_{0.9}Pr_{0.1}Fe_{0.9}Ti_{0.1}O_3$), which indicates the reduction of its ferroelectric nature and suppression of relaxation behavior above room temperature. Room temperature P–E loops also show that the value of polarization increases by doping and it is maximum for Pr doped ($Bi_{0.9}Pr_{0.1}FeO_3$) sample. Room temperature *M–H* curve shows slight increase in the value of magnetization from 0.071 to 0.078 emu/g after Ti and Pr co-doping. Magnetization versus temperature (*M–T*) curve shows unusual magnetization behavior for Pr doped sample due to increasing Jahn–Teller interaction by doping of Pr at Bi site.

Acknowledgments

This work has been financially supported by Department of Science and Technology (D.S.T.) Government of India, under research Project no. SR/FTP/PS-62/2008. The authors are also thankful to Director, N.I.T. Kurukshetra, for providing facilities to accomplish this work.

References

[1] B. Kundys, M. Viret, D. Colson, D.O. Kundys, Light-induced size changes in $BiFeO_3$ crystals, Nature Materials 9 (2010) 803.
[2] V. Shelke, D. Mazumdar, G. Srinivasan, A. Baddorf, A. Gupta, Reduced coercive field in $BiFeO_3$ thin films through domain engineering, Advanced Materials 23 (2011) 669.
[3] G. Catlan, J.F. Scoot, Physics and applications of bismuth ferrite, Advanced Materials 219 (2009) 2463.
[4] P. Rovillain, R. Desousa, Y. Gallais, A. Sacuto, A. Forget, M. Bibes, M. Cazayous, Electric-field control of spin waves at room temperature in multiferroic $BiFeO_3$, Nature Materials 9 (2010) 2463.
[5] T. Zhao, et al., Electrical control of antiferromagnetic domains in multiferroic, $BiFeO_3$ films at room temperature, Nature Materials 5 (2006) 823.
[6] W. Eerenstein, N.D. Mathur, J.F. Scott, Multiferroic and magnetoelectric materials, Nature 442 (2006) 759.
[7] V.S. Puli, A. Kumar, N. Panwar, R.S. Katiyar, Transition metal modified bulk $BiFeO_3$ with improved magnetization and linear magneto-electric coupling, Journal of Alloys and Compounds 509 (2011) 8283.
[8] N.M. Murari, R. Thomas, A. Winterman, R.E. Melgarejo, R.S. Katiyar, Structural, electrical, and magnetic properties of chemical solution deposited $Bi(Fe_{0.95}Cr_{0.05})O_3$ thin films on platinized silicon substrates, Journal of Applied Physics 105 (2009) 084110.
[9] F. Cui, Y.G. Zhao, L.B. Luo, J.J. Yang, H. Chang, M.H. Zhu, D. Xie, T. L. Ren, Dielectric, magnetic, and magnetoelectric properties of La and Ti codoped $BiFeO_3$, Applied Physics Letters 97 (2010) 22290Y.
[10] S.T. Zhang, Y. Zhang, M.H. Lu, C.L. Du, Y.F. Chen, Z.G. Liu, N. B. Ming, Substitution-induced phase transition and enhanced multiferroic properties of $Bi_{1-x}La_xFeO_3$ ceramics, Applied Physics Letters 97 (2010) 222904.
[11] V.A. Khomchenko, D.A. Kislev, L.K. Bdikin, V.V. Shavartsman, Crystal structure and multiferroic properties of Gd-substituted $BiFeO_3$, Applied Physics Letters 93 (2008) 262905.

[12] Y. Wang, C.W. Nan, Enhanced ferroelectricity in Ti-doped multiferroic $BiFeO_3$ thin films, Applied Physics Letters 93 (2008) 262905.
[13] Y.F. Cui, Y.G. Zhao, L.B. Luo, J.J. Yang, H. Chang, M.H. Zhu, D. Xie, T.L. Ren, Dielectric, magnetic, and magnetoelectric properties of La and Ti codoped $BiFeO_3$, Applied Physics Letters 97 (2010) 22904.
[14] M.M. Kumar, A. Srinivas, S.V. Suryanaryana, G.S. Kumar, T. Bhimasankaram, Bulletin of Materials Science 21 (1998) 251.
[15] G.L. Yuan, S.W. Or, H.L.W. Chan, Structural transformation and ferroelectric–paraelectric phase transition in $Bi_{1-x}La_xFeO_3$ ($x=0$–0.25) multiferroic ceramics, Journal of Physics D 40 (2007) 1196.
[16] D.H. Wang, W.C. Goh, M. Ning, C.H. Ong, Effect of Ba doping on magnetic, ferroelectric, and magnetoelectric properties in mutiferroic $BiFeO_3$ at room temperature, Applied Physics Letters 88 (2006) 212907.
[17] S. Goswami, D. Bhattacharya, P. Choudhury, Particle size dependence of magnetization and noncentrosymmetry in nanoscale $BiFeO_3$, Journal of Applied Physics 109 (2011) 07D737.
[18] A. Paul, The Kirkendall Effect in Solid State Diffusion, Ph.D. Thesis, 104 (18), 2004.
[19] Y. Feldman, A. Puzenko, Y. Ryabov, Dielectric relaxation phenomena in complex materials, Advances in Chemical Physics, vol. 133, John Wiley & Sons, Ltd, 2006, pp. 1–125.
[20] J. Liu, C.G. Duan, W.G. Yin, W.N. Mei, J.R. Hardy, Large dielectric constant and Maxwell–Wagner relaxation in $Bi_{2/3}Cu_3Ti_4O_{12}$, Physical Review B 70 (2004) 144106.
[21] S. Hunpratub, P. Thongbai, T. Yamwong, R. Yimnirun, S. Maensiri, Dielectric relaxation and dielectric response in multiferroic $BiFeO_3$ ceramics, Applied Physics Letters 94 (2009) 062904.
[22] A. Ianculescu, F.P. Gheorghiu, P. Postolache, The role of doping on the structural and functional properties of $BiFe_{1-x}Mn_xO_3$ magnetoelectric ceramics, Journal of Alloys and Compounds 504 (2010) 420.
[23] Y. Yao, W. Liu, Y. Chan, C. Leung, C. Mak, Studies of rare-earth-doped $BiFeO_3$ ceramics, International Journal of Applied Ceramic Technology 8 (5) (2011) 1246.
[24] N. Jeon, D. Rout, W. Kim, S.J.L. Kang, Enhanced multiferroic properties of single-phase $BiFeO_3$ bulk ceramics by Ho doping, Applied Physics Letters 98 (2011) 072901.
[25] L.H. Yin, Y.P. Sun, F.H. Zhang, W.B. Wu, X. Luo, X.B. Zhu, Z. R. Yang, J.M. Dai, Magnetic and electrical properties of $Bi_{0.8}Ca_{0.2}Fe_{1-x}Mn_xO_3$ ($0\leq x\leq 0.5$), Journal of Alloys and Compounds 488 (2009) 254.
[26] G.L. Yuan, S.W. Or, J.M. Liu, Z.G. Liu, Structural transformation and ferroelectromagnetic behavior in single-phase $Bi_{1-x}Nd_xFeO_3$ multiferroic ceramics, Applied Physics Letters 89 (2006) 052905.
[27] A.V. Zalesskii, A.A. Frolov, T.A. Khimich, A.A. Bush, Composition induced transition of spin modulated structure into a uniform magnetic state in a $Bi_{1-x}La_xFeO_3$, Physics of the Solid State 45 (2003) 143.
[28] I. Sosnowska, T. Peterlin-Neumaier, E. Streichele, Spiral magnetic ordering in bismuth ferrite, Journal of Physics C 15 (1982) 4835.
[29] Y.Q. Lin, X.M. Chen, Dielectric, ferromagnetic characteristics and room temperature magnetodielectic effects in double perovskite La_2CoMnO_6 ceramics, Journal of the American Ceramic Society 94 (3) (2001) 782.
[30] A.K. Pradhan, Kai Zhang, D. Hunter, J.B. Dadson, G.B. Loiutts, P. Bhattacharya, R. Katiyar, Jun Zhang, D.J. Sellmyer, U.N. Roy, Y. Cui, A. Burger, Magnetic and electrical properties of single-phase multiferroic $BiFeO_3$, Journal of Applied Physics 97 (2005) 093903.